Letter | Editors' Suggestion

Stability of particle clusters bound by capillary bridges in extensional flow

Sagar Chaudhary
Department of Mechanical Science and Engineering, and Beckman Institute for Advanced Science and Technology, University of Illinois at Urbana-Champaign, Urbana, Illinois 61801, USA

Dimitrios Fraggedakis* and Charles M. Schroeder†
Department of Chemical and Biological Engineering, Princeton University, Princeton, New Jersey 08540, USA

(Received 29 August 2025; accepted 30 January 2026; published 17 March 2026)

Capillary suspensions are commonly encountered in a wide array of applications, but their stability in flow is not fully understood. Here, we investigate the stability of a two-particle capillary cluster in extensional flow using a combination of theory and experiments. A linear stability analysis reveals the existence of a critical capillary number $\mathrm{Ca}_c = (8/45)\cos\theta$ that depends only on the contact angle θ. For $\mathrm{Ca} > \mathrm{Ca}_c$, clusters are unconditionally unstable, regardless of initial conditions. For $\mathrm{Ca} < \mathrm{Ca}_c$, a nonlinear analysis shows the existence of a Ca-dependent minimum interparticle separation beyond which breakup occurs. The analytical model further supports the experimentally observed slowdown in relaxation dynamics. Theoretical predictions are supported by precise flow experiments using a Stokes trap, where active flow modulation is used to stabilize an initially unstable cluster in extensional flow. Overall, these results provide a quantitative understanding of capillary suspension stability in flow.

DOI: 10.1103/g9nd-jlc9

Capillary suspensions consist of solid particles held together by a dispersed fluid phase in a second continuous, immiscible fluid phase. Liquid bridges between particles give rise to attractive capillary forces, resulting in percolating networks even at low solid volume fractions [1]. Complex microstructural interactions in these materials ultimately cause dramatic changes in rheological properties such as the emergence of yield stress and elasticity [2–4]. Capillary suspensions are widely encountered in industrial applications, including the formulation of stable food emulsions [5], lightweight and crack-resistant construction materials [6], macroporous ceramics for filtration and catalysis [7–9], and printable pastes for electronics and energy devices [10–14]. Despite recent progress, we lack a fundamental understanding of flow-induced instabilities in capillary suspensions, especially under extensional deformations [15,16].

A two-particle cluster bound by a liquid bridge is the simplest cohesive unit in a capillary suspension. The fundamental structure of a particle doublet serves as a building block for more complex networks and offers a minimal yet insightful system to understand the dynamics in flow [17]. Prior work has focused on characterizing the equilibrium properties of capillary bridges, including experimental measurement of static adhesion forces between a sphere and a flat plate [18] or between two stationary spheres connected by a liquid bridge [19,20]. Capillary bridges between moving particles were studied using displacement-controlled setups, revealing force-displacement

*Contact author: dfrag@princeton.edu
†Contact author: cschroeder@princeton.edu

profiles and rupture distances [21–23]. A significant body of theoretical and numerical work has also focused on understanding and predicting capillary bridge shapes and forces in equilibrium or quasi-static regimes as a function of bridge volume, particle size, and contact angle [24–34].

Capillary suspensions encounter strong flows during processing applications such as printing or extrusion. Capillary bridges can deform or rupture depending on the flow type, e.g., shear flow or extensional flow. Simple shear flow can be decomposed into equal contributions of extension and rotation [35], with the extensional component leading to dominant stretching behavior. In contrast to droplet systems, where deformable interfaces can merge through film drainage and coalescence under flow [36], the present study focuses on rigid particles joined by a liquid bridge of fixed volume, for which coalescence is precluded. These distinctions highlight the different physical regimes of capillary-mediated interactions explored here versus interfacial coalescence in deformable droplets. Flow alters particle network morphology, yet the mechanisms controlling capillary cluster behavior remain unclear.

In this Letter, we study the stability of particle clusters in extensional flow using a combination of theory and experiments. Our work directly addresses several key scientific questions, including: is there a critical flow rate above which clusters are unconditionally unstable? Does particle cluster stability depend on conformation or liquid bridge volume below the critical deformation rate? We determine a critical deformation rate governing the stability of particle clusters in flow. Our analysis further reveals the existence of a flow-rate-dependent minimum interparticle separation beyond which breakup occurs.

Experiments. We experimentally investigated the dynamics of a two-particle cluster held together by a liquid bridge in extensional flow. Materials were selected using a density-matching condition (Supplemental Material [37]). We focus on a two-particle cluster that is initially localized near the center of a cross-slot microfluidic device using a Stokes trap [38–42]. All experiments are performed in the limit of low particle Reynolds number, $\mathrm{Re}_p = \rho_c R U/\eta_c \approx 10^{-7}$, and device Reynolds number, $\mathrm{Re}_d = \rho_c H U/\eta_c \approx 10^{-6}$, where R is the particle radius, H is the channel height, ρ_c is the suspending fluid density, η_c is the suspending fluid viscosity, and U is a characteristic velocity. Figure 1(a) shows a schematic of the experimental setup with a four-channel microfluidic device. A planar extensional flow is imposed at $\widetilde{t} = 0$ s, and the temporal evolution of the minimum distance $\widetilde{D}_s$ (in micrometers) between the surfaces of the two particles is tracked as a function of time [Fig. 1(b)]. The dimensionless parameter that quantifies the strength of the imposed flow field, and thus cluster dynamics, is the capillary number $\mathrm{Ca} = \dot{\epsilon} R \eta_c/\gamma$, which measures the ratio of viscous to surface tension forces due to an externally imposed extensional rate $\dot{\epsilon}$.

We first consider cluster dynamics for $\mathrm{Ca} = 0.031$. Although the particles are initially at close proximity, $\widetilde{D}_s$ starts increasing around $\widetilde{t} \simeq 30$ s, ultimately leading to pinch-off of the capillary bridge and complete particle separation [Fig. 1(c)]. The experiment was then repeated, but under a relatively weaker imposed extension rate corresponding to $\mathrm{Ca} = 0.024$. In these conditions, we find that the cluster remains stable for all times examined.

These results show that small differences in the extension rate $\dot{\epsilon}$ lead to qualitatively distinct outcomes in transient deformation trajectories of particle clusters. Several key questions naturally arise associated with the behavior of capillary suspensions in flow: does there exist a critical capillary number Ca_c above which the two-particle cluster will break up? Are particle clusters unconditionally stable for $\mathrm{Ca} \leqslant \mathrm{Ca}_c$, or does cluster stability depend on additional material properties and/or preparation conditions? To answer these questions, we proceed with an analytical model for cluster dynamics.

Theory. We use an analytical model describing the evolution of the minimum distance between the surfaces of the two particles [17]. This model incorporates the effects of capillary forces from the liquid bridge, lubrication forces at close approach, and hydrodynamic drag due to the applied extensional flow and long-range hydrodynamic interactions (HI) between the particles. Notably, the analytical model incorporates the first-order correction to the HI-induced disturbance velocities, per the method of reflections [43], providing a simplified yet realistic approximation for flow-induced HI between particles. As a result, the overall force balance for each particle

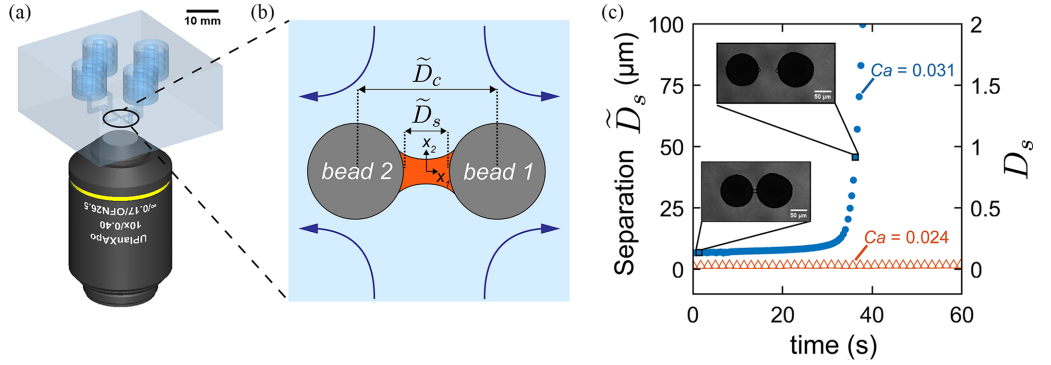

FIG. 1. Particle cluster dynamics and stability in extensional flow. (a) Schematic of experimental setup showing 3D-printed, four-channel microfluidic cross-slot device along with a 10× magnification air-immersion objective lens. The height and width of the microdevice channels are 1 mm, and the four channels are connected to fluid reservoirs pressurized by regulators and controlled using a custom labview program [17]. The cross-slot geometry generates a planar extensional flow, and the open surface of the device is sealed with a glass coverslip for optical microscopy. (b) Schematic of a two-particle cluster in the microfluidic device trapped near the stagnation point in planar extensional flow. The shear viscosities of the continuous and meniscus fluids were $\eta_c = 10\,\mathrm{Pa\,s}$ and $\eta_d = 19\,\mathrm{Pa\,s}$, respectively, resulting in a viscosity ratio $\eta^0 = \eta_d/\eta_c = 1.9$. The meniscus fluid is immiscible with the continuous phase fluid and wets the particles with an average contact angle $\theta = 55^\circ \pm 4^\circ$. (c) Transient stretching dynamics showing interparticle separation $\widetilde{D}_s$ as a function of time for two-particle clusters in planar extensional flow. Two different experiments are shown at different capillary numbers corresponding to $\mathrm{Ca} = 0.031$ (blue circles) and $\mathrm{Ca} = 0.024$ (orange triangles). Inset: Brightfield microscopy image of a liquid-bound two-particle cluster in planar extensional flow. Deformation of liquid bridges in extensional flow leads to interparticle separation and eventual breakup.

is $\mathbf{F}^i_{\mathrm{cap}} + \mathbf{F}^i_{\mathrm{lub}} + \mathbf{F}^i_{\mathrm{drag}} = \mathbf{0}$, where i denotes the particle index. These considerations lead to the following evolution equation for the dimensionless minimum distance D_s between the particles:

$$\zeta(D_s)\frac{dD_s}{dt} = f_{\mathrm{drag}}(D_s) + f_{\mathrm{cap}}(D_s), \tag{1a}$$

with

$$f_{\mathrm{drag}}(D_s) = 3\mathrm{Ca}\left(D_c - \frac{5}{D_c^2} + \frac{3}{D_c^4}\right) \tag{1b}$$

and

$$f_{\mathrm{cap}}(D_s) = \left[1 - \frac{\sqrt{\pi}D_s}{\sqrt{2V + \pi D_s^2}}\right]\left(\frac{3}{D_c} - 2\right)\cos\theta, \tag{1c}$$

where θ is the wetting fluid-solid contact angle and V is the dimensionless liquid bridge volume. Here, $\zeta(D_s) \equiv 6F(D_s)/[D_s K^2(D_s)]$ is an effective friction coefficient on the particle doublet as a result of the lubrication forces [44], with $F(D_s) = D_s K(D_s) + [K(D_s) - D_s][\eta^0 K(D_s) + D_s(1 - \eta^0)]$; $K(D_s) = \sqrt{V/\pi + D_s^2}$ is a dimensionless function of V and D_s; and $\eta^0 = \eta_d/\eta_c$ is the relative viscosity between the meniscus and continuous phase fluids. As shown in Fig. 1(b), $\widetilde{D}_c$ is the center-to-center distance and $\widetilde{D}_s$ is the smallest separation between the particle surfaces such that $\widetilde{D}_c = \widetilde{D}_s + 2R$, where D_c, D_s, and V are the dimensionless forms of $\widetilde{D}_c$, $\widetilde{D}_s$, and $\widetilde{V}$, respectively. All quantities in Eq. (1) are expressed in their dimensionless form using R, the particle radius, and $\tau_c = R\eta_c/\gamma$ as the characteristic length and time scales, respectively. Additional details on the derivation of Eq. (1) are provided in the Supplemental Material [37].

Before proceeding, we comment on the nature and behavior of the dissipative terms in the evolution equation. First, we observe that $\zeta(D_s)^{-1} \sim D_s$, and as a consequence, $\zeta(D_s)$ diverges as $D_s \to 0$ due to the increasing dynamic pressure in the gap between particles upon close approach. Additionally, f_{drag} results from the superposition of the undisturbed velocity and disturbance velocity fields due to interparticle HI. A key aspect in quantitatively capturing the evolution of D_s is the competition between f_{cap} and the drag arising from the disturbance velocity fields [17].

Linear stability analysis. To determine the criteria for particle cluster breakup in extensional flow, we recast Eq. (1a) as $dD_s/dt = (f_{\text{drag}} + f_{\text{cap}})/\zeta$ and seek steady solutions by setting $dD_s/dt = 0$, which are then analyzed with respect to their stability. One can readily show that $D_{s,r_1} = 0$ satisfies Eq. (1a) identically, which physically corresponds to the case where the two particles are in contact. To explore the stability of the trivial root to infinitesimal perturbations, the ansatz $D_s(t) = D_{s,r_1} + \delta D_s(t)$ is inserted into Eq. (1a), and the limit $\delta D_s(t) \to 0$ is considered, resulting in an evolution equation for the fluctuations:

$$\frac{d\delta D_s}{dt} = \frac{(45\text{Ca} - 8\cos\theta)}{96\eta^0}\delta D_s. \tag{2}$$

Equation (2) has solutions of the form $\delta D_s(t) = \delta D_0 e^{\sigma t}$, with the growth factor $\sigma = (45\text{Ca} - 8\cos\theta)/96\eta^0$.

The sign of σ determines the stability of the meniscus to infinitesimal perturbations; in particular, when $\sigma > 0$, any perturbations will grow exponentially, whereas for $\sigma < 0$, the perturbations will decay. Thus, the marginal stability curve, i.e., $\sigma = 0$, is given by

$$\text{Ca}_\text{c} = \tfrac{8}{45}\cos\theta, \tag{3}$$

where Ca_c is the critical capillary number above which two-particle clusters are unstable under extensional flow regardless of initial conditions. For the experimental system of Fig. 1, where $\theta = 55^\text{o}$, we find $\text{Ca}_\text{c} \approx 0.1$. Comparing this value to the experimental conditions of Fig. 1(c), we find that Ca_c is approximately three times larger than the operating conditions of $\text{Ca} = 0.031$ for which we observe the breakup of the two-particle cluster.

Although it appears that Ca_c is larger than the Ca for particle breakup based on the experiments in Fig. 1, this apparent contradiction can be reconciled by considering the possibility that the particles do not initially start from $D_s(t = 0) = 0$ when the flow is imposed. In fact, it is unlikely that the initial distance between the particles would be $D_s = 0$, as surface-to-surface contact corresponds to the asymptotic result expected by allowing the two-particle cluster to relax in the presence of lubrication forces for $t \to \infty$. Based on these arguments, we further examined the nonlinear behavior of dD_s/dt as predicted by Eq. (1) for different initial conditions.

Initial condition-dependent cluster stability. We next examine the possibility of a stability criterion for capillary suspensions that explicitly depends on the initial D_s between the two particles in the cluster. We consider Eq. (1) and examine the value of $dD_s/dt|_{t=0}$ for different initial conditions $D_s(t = 0)$. Here, f_{cap}, f_{drag}, and ζ depend explicitly on Ca, the volume of the liquid bridge V, and the viscosity ratio η^0, for which we use numerical values from the experiments in Fig. 1(c), namely, $V = 0.012$, $\eta^0 = 1.9$, and $\text{Ca} = 0.031$.

Figure 2(a) shows the variation of $dD_s/dt|_{t=0}$ as a function of $D_s(t = 0)$ for three Ca values. Clearly $dD_s/dt|_{t=0}$ has two roots: one root at $D_{s,r_1} = 0$ and a second root $D_{s,r_2} > 0$. The case of the trivial root $D_{s,r_1} = 0$ was considered for the linear stability analysis, and we now focus on the behavior around the second root D_{s,r_2}. For $0 < D_s < D_{s,r_2}$, we find that $dD_s/dt < 0$. Therefore, for all initial separations where $D_s(0) < D_{s,r_2}$, the interparticle separation distance should relax to D_{s,r_1}, and thus the cluster should not break up if $\text{Ca} < \text{Ca}_\text{c}$. However, for $D_s(0) > D_{s,r_2}$, even though $\text{Ca} < \text{Ca}_\text{c}$, $dD_s/dt > 0$, which leads to eventual cluster breakup. Interestingly, when $\text{Ca} \to \text{Ca}_\text{c}$, the two roots merge, i.e., $D_{s,r_2} \to D_{s,r_1}$, supporting the claim that Eq. (3) provides the critical Ca above which two-particle clusters are always unstable.

Figure 2(b) summarizes the particle cluster stability behavior in terms of a phase diagram expressed as a function of Ca versus $D_s(0)$. The critical line (solid black line) corresponds to the

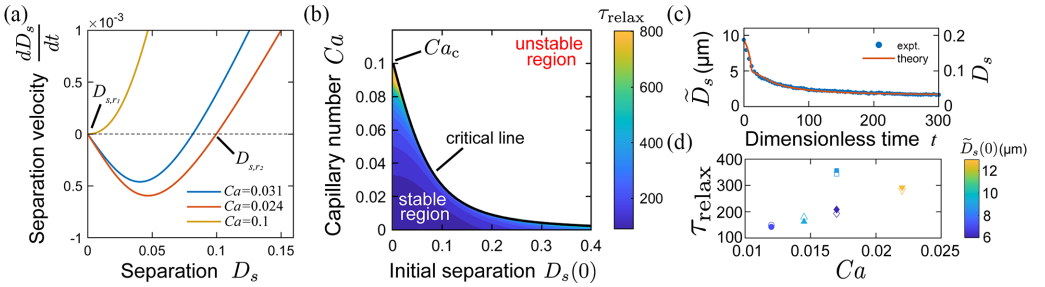

FIG. 2. Nonlinear analysis and dynamics for two-particle clusters in extensional flow. (a) Interparticle separation velocity dD_s/dt as a function of interparticle separation D_s for three Ca values and $V = 0.012$, revealing two roots of the equation $dD_s/dt = 0$. For the critical value $\mathrm{Ca_c} = 0.1$, both roots merge at $D_s = 0$. (b) Phase diagram for particle cluster stability showing stable and unstable regions by plotting Ca as a function of initial separation distance $D_s(0)$. The phase diagram shows the critical capillary number line $\mathrm{Ca_c}(D_{s,r_2})$ and dimensionless relaxation times for various Ca values below the critical line, corresponding to particle cluster relaxation under finite Ca such that $\mathrm{Ca} < \mathrm{Ca_c}$. (c) Transient relaxation trajectories of particle clusters by plotting interparticle separation $\widetilde{D}_s$ (or D_s) as a function of dimensionless time t during cluster relaxation for $\mathrm{Ca} = 0.015$. (d) Cluster relaxation times from experiment and theory for various Ca values below the critical value. Each filled data point represents a two-particle cluster experiment, and the unfilled data points of the same shape represent the theoretical relaxation times. Different marker shapes show different liquid-bridge volumes: ◯: 1500 μm^3, △: 2000 μm^3, ◇: 2200 μm^3, □: 1300 μm^3, ▽: 3000 μm^3. The color bar represents the initial separation distance $\widetilde{D}_s(0)$ of the cluster when it begins to relax; the final separation for all experiments lies between 2 and 4 μm.

locus of $\mathrm{Ca_c}(D_{s,r_2})$ and shows that $\mathrm{Ca_c}$ decreases with increasing $D_s(0)$. This result can be physically understood from the perspective that smaller extensional rates are required to separate a cluster in which the two particles are further apart compared to the case where the particles are closer together. Additionally, as the critical line approaches the close-contact limit, $\mathrm{Ca_c}(D_{s,r_2}) \to \mathrm{Ca_c}$, and we recover $\mathrm{Ca_c} = 8\cos\theta/45 \approx 0.1$.

The nonlinear analysis clearly explains how initial conditions affect cluster stability based on experimental observations shown in Fig. 1(c), where two different particle clusters subjected to Ca values less than $\mathrm{Ca_c}$ show qualitatively different behavior. Cluster 1 at $\mathrm{Ca} = 0.031$ separates and eventually breaks up in flow, whereas cluster 2 at $\mathrm{Ca} = 0.024$ remains stable in extensional flow without breaking up. The nonlinear analysis shows that for cluster 1, $D_s(0) > D_{s,r_2}$, even though $\mathrm{Ca} < \mathrm{Ca_c}$, which leads to breakup. On the other hand, for cluster 2, $D_s(0) < D_{s,r_2}$ and thus $dD_s/dt < 0$, which results in a stable particle cluster in extensional flow.

Relaxation timescales and programmable capillary break up. We further studied the relaxation times τ_{relax} of two-particle clusters located within the stable regime of the flow phase diagram [Fig. 2(b)]. We define τ_{relax} as the characteristic time required for $D_s(\tau_{\mathrm{relax}})$ to reach 10% of its initial value $D_s(0)$. Figure 2(b) shows τ_{relax}, in a contour plot format, for all stable initial distances that the particles can have for different values of Ca. For small Ca, τ_{relax} decreases as a result of the smaller extensional forces counteracting the retraction forces due to the liquid bridge between the particles. On the other hand, our results show a slowing down in the cluster relaxation dynamics for $\mathrm{Ca} \to \mathrm{Ca_c}(D_{s,r_2})$, as τ_{relax} increases to larger values. This behavior can be qualitatively understood by examining the dynamics near D_{s,r_1}, described by Eq. (2). In particular, for $\delta D_s(\tau_{\mathrm{relax}}) = 0.1\,\delta D_0$, we obtain $\tau_{\mathrm{relax}} \sim |\mathrm{Ca} - \mathrm{Ca_c}|^{-1}$, which shows that $\tau_{\mathrm{relax}} \to \infty$ as $\mathrm{Ca} \to \mathrm{Ca_c}$. The predicted behavior indicates that one should expect a critical slowdown as we approach the universally predicted $\mathrm{Ca_c}$. Along the same lines, a qualitatively similar behavior is found for the dynamics close to D_{s,r_2}, as supported by the experimental observations and numerical solution of Eq. (1a) shown in Fig. 2(d).

The theoretical predictions of τ_{relax} were validated by conducting two-particle cluster relaxation experiments at finite Ca values (see Supplemental Material [37]). In capillary suspensions, two

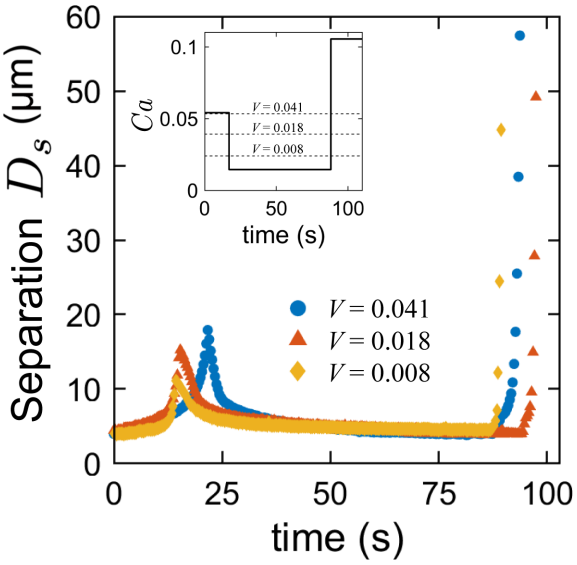

FIG. 3. Transient stretching, relaxation, and restretching experiments on three different two-particle clusters with different liquid bridge volumes V in extensional flow using a Stokes trap. Particle clusters are first stretched to a finite interparticle separation distance before breakup and then allowed to relax to the initial separation at $\mathrm{Ca} = 0.015$. Following relaxation, the capillary number is increased to $\mathrm{Ca} > \mathrm{Ca_c}$, which induces particle cluster breakup. The inset shows the flow-rate program of Ca as a function of time that is applied using automated flow control via the Stokes trap. The thin dashed lines in the inset show the critical capillary numbers $\mathrm{Ca_c}(D_{s,r_2})$ for the particle clusters with the respective bridge volumes V in these experiments.

closely spaced and approaching particles tend to relax to a steady state with a small but finite interparticle separation due to surface roughness or excluded volume effects [45–48]. This phenomenon is accounted for by including a repulsive force of the Weeks-Chandler-Andersen-type (WCA) (see Supplemental Material [37]) [17].

Results from cluster relaxation experiments and the analytical model are shown in Fig. 2(c), which plots the relaxation of $\widetilde{D}_s$ (or D_s) as a function of dimensionless time t under an imposed extensional flow at $\mathrm{Ca} = 0.015$. This experiment was repeated for different Ca values and initial conditions. Figure 2(d) shows the dimensionless relaxation times τ_{relax} as a function of Ca for a series of particle cluster relaxation experiments in weak flow ($\mathrm{Ca} < \mathrm{Ca_c}(D_{s,r_2})$). Predictions from the models of Eq. (1) are also shown in Fig. 2(d). Overall, good agreement is observed between experiments and theory for cluster relaxation times under finite Ca. We note that including the WCA force in the model does not alter the stability results because at critical distances for cluster breakup, the particles are generally far apart and the interparticle repulsive forces are negligible.

We next performed a series of experiments to demonstrate the predictive power of the theory related to $\mathrm{Ca_c}(D_{s,r_2})$ (Fig. 3). As shown in the inset of Fig. 3, a two-particle doublet is deformed to an arbitrary interparticle separation, followed by rapidly reducing the Ca to a value $\mathrm{Ca} < \mathrm{Ca_c}(D_{s,r_2})$. The cluster is then allowed to relax to the same initial separation $\widetilde{D}_s(0)$. Following cluster relaxation, the Ca value is increased to a value slightly above $\mathrm{Ca_c} \approx 0.1$. In all cases, regardless of initial conditions or bridge volume, cluster breakup is observed in the third phase of the experiment. These observations confirm the theoretical predictions regarding $\mathrm{Ca_c}$ for the close contact or near-zero separation state. These results also demonstrate the ability to manipulate cluster stability on the fly, enabling active control of capillary clusters.

In this Letter, we determined a critical capillary number $\mathrm{Ca_c}$ for cluster breakup describing the limit of stability in the close-contact regime that depends only on the contact angle θ. For

$\mathrm{Ca} < \mathrm{Ca}_c$, a nonlinear analysis reveals the existence of a Ca-dependent minimum interparticle separation beyond which breakup occurs, consistent with experimental observations. Our results demonstrate the predictive power of the theory and establish an approach for actively controlling capillary cluster stability using flow, with implications for the design and processing of capillary suspensions in materials applications.

Acknowledgments. We thank Professor Sachin S. Velankar for useful discussions. This work was supported by the National Science Foundation under Grant No. CBET-2030537. D.F. acknowledges Princeton University and the Department of Chemical and Biological Engineering for financial support provided through start-up funding.

Data availability. The data that support the findings of this article are not publicly available upon publication because it is not technically feasible and/or the cost of preparing, depositing, and hosting the data would be prohibitive within the terms of this research project. The data are available from the authors upon reasonable request.

[1] E. Koos and N. Willenbacher, Capillary forces in suspension rheology, Science **331**, 897 (2011).
[2] S. Van Kao, L. E. Nielsen, and C. T. Hill, Rheology of concentrated suspensions of spheres. II. Suspensions agglomerated by an immiscible second liquid, J. Colloid Interface Sci. **53**, 367 (1975).
[3] E. Koos, Capillary suspensions: Particle networks formed through the capillary force, Curr. Opin. Colloid Interface Sci. **19**, 575 (2014).
[4] E. Koos, J. Johannsmeier, L. Schwebler, and N. Willenbacher, Tuning suspension rheology using capillary forces, Soft Matter **8**, 6620 (2012).
[5] S. Hoffmann, E. Koos, and N. Willenbacher, Using capillary bridges to tune stability and flow behavior of food suspensions, Food Hydrocoll. **40**, 44 (2014).
[6] M. Schneider, J. Maurath, S. B. Fischer, M. Weiß, N. Willenbacher, and E. Koos, Suppressing crack formation in particulate systems by utilizing capillary forces, ACS Appl. Mater. Interfaces **9**, 11095 (2017).
[7] J. Dittmann, E. Koos, and N. Willenbacher, Ceramic capillary suspensions: Novel processing route for macroporous ceramic materials, J. Am. Ceram. Soc. **96**, 391 (2013).
[8] A. R. Studart, U. T. Gonzenbach, E. Tervoort, and L. J. Gauckler, Processing routes to macroporous ceramics: A review, J. Am. Ceram. Soc. **89**, 1771 (2006).
[9] M. Weiß, P. Sälzler, N. Willenbacher, and E. Koos, 3D-printed lightweight ceramics using capillary suspensions with incorporated nanoparticles, J. Eur. Ceram. Soc. **40**, 3140 (2020).
[10] S. Roh, D. P. Parekh, B. Bharti, S. D. Stoyanov, and O. D. Velev, 3D printing by multiphase silicone/water capillary inks, Adv. Mater. **29**, 1701554 (2017).
[11] D. Amoabeng and S. S. Velankar, Bulk soldering: Conductive polymer composites filled with copper particles and solder, Colloids Surf. A **553**, 624 (2018).
[12] M. Schneider, E. Koos, and N. Willenbacher, Highly conductive, printable pastes from capillary suspensions, Sci. Rep. **6**, 31367 (2016).
[13] J. Yang, Z. Hu, H. Yan, and F. Niu, Magnetorheological suspension with capillary network, J. Intell. Mater. Syst. Struct. **30**, 1850 (2019).
[14] D. Menne, L. Lemos da Silva, M. Rotan, J. Glaum, M. Hinterstein, and N. Willenbacher, Giant functional properties in porous electroceramics through additive manufacturing of capillary suspensions, ACS Appl. Mater. Interfaces **14**, 3027 (2022).
[15] K. Hauf and E. Koos, Structure of capillary suspensions and their versatile applications in the creation of smart materials, MRS Commun. **8**, 332 (2018).
[16] F. Bossler, L. Weyrauch, R. Schmidt, and E. Koos, Influence of mixing conditions on the rheological properties and structure of capillary suspensions, Colloids Surf. A **518**, 85 (2017).
[17] S. Chaudhary, S. S. Velankar, and C. M. Schroeder, Dynamics of meniscus-bound particle clusters in extensional flow, J. Rheol. **68**, 397 (2024).

[18] J. S. McFarlane and D. Tabor, Adhesion of solids and the effect of surface films, Proc. R. Soc. Lond. A **202**, 224 (1950).
[19] G. Mason and W. Clark, Liquid bridges between spheres, Chem. Eng. Sci. **20**, 859 (1965).
[20] C. D. Willett, M. J. Adams, S. A. Johnson, and J. P. Seville, Capillary bridges between two spherical bodies, Langmuir **16**, 9396 (2000).
[21] O. Pitois, P. Moucheront, and X. Chateau, Liquid bridge between two moving spheres: An experimental study of viscosity effects, J. Colloid Interface Sci. **231**, 26 (2000).
[22] M. Bozkurt, D. Fratta, and W. Likos, Capillary forces between equally sized moving glass beads: An experimental study, Can. Geotech. J. **54**, 1300 (2017).
[23] D. Lievano, S. Velankar, and J. J. McCarthy, The rupture force of liquid bridges in two and three particle systems, Powder Technol. **313**, 18 (2017).
[24] R. Fisher, On the capillary forces in an ideal soil; correction of formulae given by W.B. Haines, J. Agric. Sci. **16**, 492 (1926).
[25] B. Derjaguin, Untersuchungen ueber die reibung und adhaesion, IV: Theorie des anhaftens kleiner teilchen, Kolloid-Z. **69**, 155 (1934).
[26] J. N. Israelachvili, Surface forces, *The Handbook of Surface Imaging and Visualization* (CRC Press, Boca Raton, 2022), pp. 793–816.
[27] Y. I. Rabinovich, M. S. Esayanur, and B. M. Moudgil, Capillary forces between two spheres with a fixed volume liquid bridge: Theory and experiment, Langmuir **21**, 10992 (2005).
[28] H.-J. Butt and M. Kappl, Normal capillary forces, Adv. Colloid Interface Sci. **146**, 48 (2009).
[29] G. Lian, C. Thornton, and M. J. Adams, A theoretical study of the liquid bridge forces between two rigid spherical bodies, J. Colloid Interface Sci. **161**, 138 (1993).
[30] C.-F. Zhao, N. P. Kruyt, and O. Millet, Capillary bridges between spherical particles under suction control: Rupture distances and capillary forces, Powder Technol. **360**, 622 (2020).
[31] L. Yang, M. Sega, and J. Harting, Capillary-bridge forces between solid particles: Insights from lattice Boltzmann simulations, AIChE J. **67**, e17350 (2021).
[32] D. Wu, P. Zhou, G. Wang, B. Zhao, T. Howes, and W. Chen, Modeling of capillary force between particles with unequal contact angle, Powder Technol. **376**, 390 (2020).
[33] M. Dörmann and H.-J. Schmid, Simulation of capillary bridges between particles, Procedia Eng. **102**, 14 (2015).
[34] M. Bagheri, S. Roy, and T. Pöschel, Approximate expressions for the capillary force and the surface area of a liquid bridge between identical spheres, Comput. Part. Mech. **11**, 2179 (2024).
[35] L. G. Leal, *Advanced Transport Phenomena: Fluid Mechanics and Convective Transport Processes* (Cambridge University Press, Cambridge, 2010).
[36] N. Bremond, A. R. Thiam, and J. Bibette, Decompressing emulsion droplets favors coalescence, Phys. Rev. Lett. **100**, 024501 (2008).
[37] See Supplemental Material at http://link.aps.org/supplemental/10.1103/g9nd-jlc9 for Materials and Methods (Sec. I), Derivation of the analytical model for cluster breakup (Sec. II), Weeks Chandler Anderson (WCA) Potential (Sec. III), Figures for relaxation dynamics (Sec. IV), Meniscus volume calculation (Sec. V), Cluster breakup movie (Sec. VI), Closed-form expression for $\mathrm{Ca_c}(\mathrm{D}_{s,r_2})$ (Sec. VII), and the Effect of bridge volume and contact angle on $\mathrm{Ca_c}(\mathrm{D}_{s,r_2})$ (Sec. VIII).
[38] A. Shenoy, C. V. Rao, and C. M. Schroeder, Stokes trap for multiplexed particle manipulation and assembly using fluidics, Proc. Natl. Acad. Sci. USA **113**, 3976 (2016).
[39] D. Kumar, A. Shenoy, S. Li, and C. M. Schroeder, Orientation control and nonlinear trajectory tracking of colloidal particles using microfluidics, Phys. Rev. Fluids **4**, 114203 (2019).
[40] A. Shenoy, D. Kumar, S. Hilgenfeldt, and C. M. Schroeder, Flow topology during multiplexed particle manipulation using a Stokes trap, Phys. Rev. Appl. **12**, 054010 (2019).
[41] D. Kumar, A. Shenoy, J. Deutsch, and C. M. Schroeder, Automation and flow control for particle manipulation, Curr. Opin. Chem. Eng. **29**, 1 (2020).
[42] M. Q. Tu, H. V. Nguyen, E. Foley, M. I. Jacobs, and C. M. Schroeder, 3D manipulation and dynamics of soft materials in 3D flows, J. Rheol. **67**, 877 (2023).

[43] S. Kim and S. J. Karrila, *Microhydrodynamics: Principles and Selected Applications* (Dover, New York, 2005).
[44] R. Lopez, J. Vaswani, D. T. Butler, J. McCarthy, and S. S. Velankar, Low viscosity liquid bridges: Stretching of liquid bridges immersed in a higher viscosity liquid, JCIS Open **9**, 100079 (2023).
[45] S. P. Kumar, A. Vázquez-Quesada, and M. Ellero, A conservative lubrication dynamics method for the simulation of dense non-colloidal suspensions with particle spin, J. Comput. Phys. **427**, 110001 (2021).
[46] D. Dratler and W. Schowalter, Dynamic simulation of suspensions of non-Brownian hard spheres, J. Fluid Mech. **325**, 53 (1996).
[47] A. Sierou and J. F. Brady, Rheology and microstructure in concentrated noncolloidal suspensions, J. Rheol. **46**, 1031 (2002).
[48] J. F. Brady and G. Bossis, The rheology of concentrated suspensions of spheres in simple shear flow by numerical simulation, J. Fluid Mech. **155**, 105 (1985).